AIP Advances

Modelling of the vertical deflection of ferroelectric bending tongues loaded at their free end

Cite as: AIP Advances **9**, 025017 (2019); https://doi.org/10.1063/1.5082392
Submitted: 21 November 2018 . Accepted: 04 February 2019 . Published Online: 14 February 2019

Juliette Cardoletti, Aldin Radetinac, Daniel Thiem, Julian Walker, Philipp Komissinskiy, Bai-Xiang Xu, Helmut Schlaak, Susan Trolier-McKinstry, and Lambert Alff

Modelling of the vertical deflection of ferroelectric bending tongues loaded at their free end

Cite as: AIP Advances 9, 025017 (2019); doi: 10.1063/1.5082392
Submitted: 21 November 2018 • Accepted: 4 February 2019 •
Published Online: 14 February 2019

Juliette Cardoletti,[1,a] Aldin Radetinac,[1] Daniel Thiem,[2] Julian Walker,[3,4] Philipp Komissinskiy,[1] Bai-Xiang Xu,[1] Helmut Schlaak,[2] Susan Trolier-McKinstry,[3] and Lambert Alff[1,b]

AFFILIATIONS

[1]Institute of Materials Science, Technische Universität Darmstadt, Alarich-Weiss-Straße 2, 64287 Darmstadt, Germany
[2]Institute of Electromechanical Design, Technische Universität Darmstadt, Merckstraße 25, 64283 Darmstadt, Germany
[3]Materials Research Institute, Pennsylvania State University, University Park, Pennsylvania 16802, USA
[4]Department of Materials Science and Engineering, Norwegian University of Science and Technology, NO-7491 Trondheim, Norway

[a]**Corresponding author:** cardoletti@oxide.tu-darmstadt.de
[b]alff@oxide.tu-darmstadt.de

ABSTRACT

In this work, a model to describe the vertical deflection of ferroelectric bending tongues with a load at their free end is proposed. The model is based on the ferroelectric switching criterion developed by Hwang *et al.* ["Ferroelectric/ferroelastic interactions and a polarization switching model," Acta Metall. Mater. **43**, 2073–2084 (1995)] and the Euler-Bernoulli beam theory. It notably takes into account the geometry of the bending tongue, the mechanical and piezoelectric material properties, the applied electrical field, the crystallographic state of the ferroelectric thin film and its built-in strain. Hwang's model is improved by incorporating strain saturation at high field, as expected for the *butterfly loop*. This allows accurate estimates of the vertical deflection for ferroelectric bending tongue based applications.

I. INTRODUCTION

With the need for miniaturization of devices and components as actuators, sensors or energy harvesters, the use of bending tongues (cantilevers or wider beams) based on piezoelectric ceramics is increasing. Due to its large piezoelectric coefficient, $PbZr_{0.52}Ti_{0.48}O_3$ (PZT) is the most commonly used material, but it is also ferroelectric (*i.e.* the polarization direction can be switched between discrete crystallographically allowed orientations by an external electric field). This particularity should be taken into account when modelling the vertical deflection of bending tongues.[1]

Though linear piezoelectric structures have been well studied, to date, very few bending tongue-based devices have been modelled by simulating the ferroelectric switching occurring in grains.[2,3] Moreover, various descriptions of ferroelectric switching have been made through micromechanical models. There are phase-field models[4–6] for polarization switching in single or multicrystals, which requires no switching criteria. Nevertheless, for polycrystalline ferroelectrics with a large amount of grains, micromechanical approaches become more efficient. Some of the micromechanical models are self-consistent estimates[7] or, in the case of Hwang *et al.*, account for hysteretic polarization-field and strain-field behavior.[8]

The latter model by Hwang *et al.* predicts the response of a bulk ferroelectric ceramic subjected to external loads, both mechanical and electrical. It describes for an individual grain the strain and polarization resulting from an

applied electrical field and applied stress. The model considers that polarization switching occurs when the loading level is larger than a work energy criterion. The response of the individual grains, which are assumed to display a statistically random orientation, is averaged to estimate the bulk response. In order to take into account more physical details, Hwang's model has been extended in various aspects, including mean-field approach, and numerically implemented with the finite-element method.[9–15]

Piezoelectric/metal/piezoelectric actuators have also been modelled by the finite-element method and laminated beam theory, taking into account static electromechanical displacement and polarization switching.[16] However, this model includes only three-point-loaded actuators.

The model described, based on Hwang's switching criterion,[8] aims to bridge the gap between the mechanical and ferroelectric approaches by describing the vertical deflection of a bending tongue fixed at one end and loaded at its free end while taking into account ferroelectric switching at the grain scale.

The proposed model includes the impact of the crystallographic state of the ferroelectric (polycrystalline, textured or epitaxial) on the vertical deflection. It also increases the accuracy of Hwang's model[8] by taking macroscopic polarization saturation into account. By analyzing in details the different contributions to the vertical deflection, the proposed model also allows optimization of the bending tongue's geometry for various applications.

II. EXTENT AND LIMITS OF THE MODELLING

A. Extent of the model

The described model applies to a composite bending tongue fixed at one end and with a width-to-depth ratio larger than 12.[17] Therefore, while Euler-Bernoulli beam theory can be used to describe its vertical deflection, it is necessary to apply corrections for both the inhomogeneity and the width of the bending tongue.

The composite bending tongue, represented in Fig. 1, is composed of three distinct layers: a ferroelectric layer, one or more buffer layers (referred to as *buffer layer* below) and a polycrystalline substrate.

The bending tongue is subjected to the gravity force of its own weight and to a load applied at its free end. The former is applied over its whole length while the latter is distributed over a certain length referred to as *length load*. Additionally, the bending tongue is subjected to both built-in strain (due to eventual misfit strain and to thermal strain) and to ferroelectric strain. The former is applied over its whole length and the latter is applied over the region where the electrodes used to activate the ferroelectric layer are located (the bending tongue's length minus the *length load*).

The bending tongue is described in a Cartesian coordinate frame, known as the *global reference frame*, where it is fixed at $x = 0$ and $z = 0$ with the x-direction along the length of the bending tongue and the bending tongue's deflection upon application of an electrical field vertically in the z-direction.

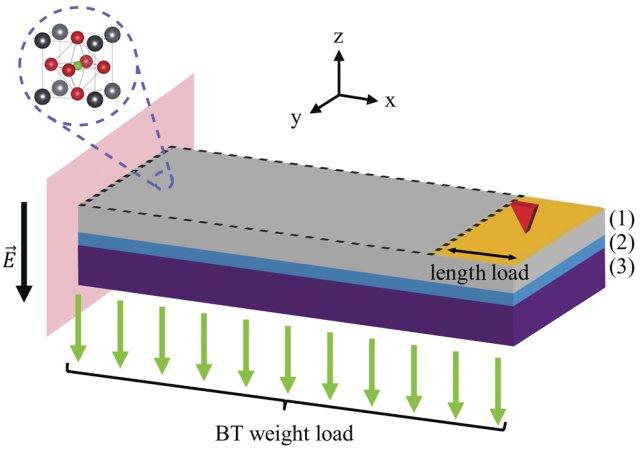

FIG. 1. Schematic representation of the modelled bending tongue (BT) in the *global reference frame* (*xyz*). The electrical field $\vec{E}$ is applied over the area delimited by dashes through all layers: (1) ferroelectric layer, (2) buffer layer(s), (3) substrate. The load at the free end (red arrow) is applied over *length load*.

As the model is aimed at functional applications, it considers four distinct states of the bending tongue: *as deposited* (before any electrical field is applied), *poled* (corresponding to the final step of the poling process, before the poling electrical field is released), *inactive* (after poling, while no electrical field is applied) and *active* (after poling, while an electrical field is applied).

B. Assumptions of the model

The model assumes several general assumptions: each individual layer composing the bending tongue is homogeneous and its properties are either isotropic or transversely isotropic in the xy-plane. The bonding between the individual layers is assumed to be perfect.

Mechanical hypotheses are also assumed in order to apply Euler-Bernoulli beam theory:[18] the composite beam has the same modulus of elasticity for both tension and compression and is presumed to be straight or slightly curved in the plane of bending (with a radius of curvature at least 10 times as long as the thickness of the bending tongue). The cross-section of the beam is assumed to be uniform along the x-axis and the bending tongue has at least one longitudinal plane of symmetry, *i.e.* the xz-plane. All loads and reactions are presumed to be perpendicular to the axis of the bending tongue, *i. e.* along the z-direction, as well as to lie in the same plane as the bending tongue which is a longitudinal plane of symmetry, *i.e.* in the xz-plane. Deformations are assumed to be small and within the range of linear elastic deformation. The bending tongue is also presumed to be long with respect to its thickness: considering it as a metal beam of compact section, its span/thickness ratio is at least equal to 8.

The model also assumes the following crystallographic assumptions: the ferroelectric layer contains only tetragonal unit cells and the substrate is polycrystalline. It is presumed that there is no phase transition in any of the materials.

Since this model is based on Hwang's model for ferroelectric switching,[8] it takes into account neither the correlation between ferroelectric domains nor domain wall motion. For such purpose, the phase field models can be utilized.[4–6] The model also considers that 180° and 90° switching requires the same amount of energy.

Due to the large number of parameters required for the modelling, the results might be strongly impacted by the selected values.

III. FUNDAMENTALS OF THE MODEL

As mentioned in section II A, the bending tongue, being a composite, requires a correction for its inhomogeneity by means of an equivalent cross-section.[18] The substrate is taken as the reference layer, implying:

$$w_{eff}^{subs} = w^{subs}, \qquad w_{eff}^{i} = w^{i}\frac{E_Y^i}{E_Y^{subs}}, \tag{1}$$

where w and w_{eff} refer to the width and the effective width of a layer, respectively, the superscripts *subs* and i refer to the substrate and any subsequent layer, respectively, and E_Y refers to the Young's modulus.

The neutral axis of the equivalent cross-section of the bending tongue and its second moment of area are impacted by taking the effective width of each layer into account. It is therefore necessary to consider the effective neutral axis, n_{eff} and the effective second moment of area I_{eff} calculated using w_{eff}.

Therefore, n_{eff}, which is also dependent on the mid-plane of each individual layer, n^i, can be expressed as:

$$n_{eff} = \frac{\sum_i w_{eff}^i t^i n^i}{\sum_i w_{eff}^i t^i}, \tag{2}$$

where t^i corresponds to the thickness of every individual layer of the bending tongue, and with n^i defined as:

$$n^i = \frac{t^i}{2} + \sum_{j=0}^{i-1} t^j. \tag{3}$$

Using Eq. 2, I_{eff} can be calculated as:

$$I_{eff} = \sum_i \frac{w_{eff}^i t^i}{12} + w_{eff}^i t^i (n^i - n_{eff})^2. \tag{4}$$

As the bending tongue is incorporated in a wide beam (width-to-depth ratio larger than 12),[17] it is also necessary to apply a correction in order to use the Euler-Bernoulli beam theory.[18] The Young's modulus of the composite beam, E_Y^{eff} should be substituted by:

$$E_Y^{eff} \rightarrow \frac{E_Y^{eff}}{1-\nu_{eff}^2}, \tag{5}$$

where ν_{eff} corresponds to the Poisson's ratio of the substrate as per the equivalent cross-section obtained from Eq. 1.

Due to both loads (the bending tongue's own weight and load applied at its free end) and strains (built-in and ferroelectric strains) acting simultaneously on the bending tongue, the equation describing its vertical deflection, Z, along the z-axis, is complex. However, the method of superposition[18] allows the total vertical deflection to be defined as the sum of the deflections due to both loads and strains. Therefore, each component of the deflection can be calculated independently.

A. Deflection due to loads

Q(x), the load distribution of the bending tongue's own weight, q^W, over its whole length and the load applied at its free end, q^L, over the *length load* can be described by the following equation using Macaulay brackets:

$$Q(x) = q^W + q^L < x - m >^0, \tag{6}$$

where m corresponds to the position on the x-axis at which *length load* begins, ranging from $x = m$ to $x = l$, the free end of the bending tongue. Macaulay brackets describe a discontinuous function expressed by the following equation:[19]

$$< x - m >^p = \begin{cases} 0 & x \le m \\ (x-m)^p & x > m \end{cases}, \tag{7}$$

where p is an integer.

According to Euler-Bernoulli beam theory, the equation describing the vertical deflection of the bending tongue can be obtained through four consecutive integrations of the load distribution over the length of the bending tongue. As the bending tongue is fixed at one end in $x = 0$ and $z = 0$, it is subjected to neither any shear force nor bending moment at its free end at which $x = l$. It also does not have a slope or a deflection at its fixed end. Therefore, the following boundary conditions can be applied:

$$Z^{III}(x = l) = 0;\ Z^{II}(x = l) = 0, \qquad Z^{I}(x = 0) = 0 \text{ and } Z(x = 0) = 0, \tag{8}$$

where Z^I, Z^{II} and Z^{III} are the first, second and third derivatives of Z, the vertical deflection.

From Eq. 6 and 8, the equation of vertical deflection due to the bending tongue's own weight and the load applied at its free end can be obtained:

$$Z = \frac{1-\nu_{eff}^2}{24E_Y^{eff}I_{eff}}\left[q^W x^4 + q^L < x - m >^4 + 4(-q^W l - q^L(l-m))x^3 + 12\left[q^W\frac{l^2}{2} + q^L(l-m)\left(l - \frac{l-m}{2}\right)\right]x^2\right]. \tag{9}$$

The detailed calculations from Eq. 6 to Eq. 9 are given in Appendix A.

B. Deflection due to strains

Both terms of the built-in strain in the ferroelectric layer (thermal strain and eventual misfit strain) as well as ferroelectric strain have components in the xy-plane and in the z-direction. However, their components in the z-direction can be neglected as the top surface of the bending tongue is free and, therefore, unconstrained.

To maintain the force equilibrium in the bending tongue, the in-plane built-in strain, ε_b, and the in-plane ferroelectric strain, ε_f generate longitudinal strains in both the x-direction and the y-direction.[20] These created strains ε_b^l and ε_f^l, respectively, are defined as:

$$\varepsilon_b^l = -\frac{E_Y^f t^f \varepsilon_b}{\sum_i E_Y^i t^i}, \qquad \varepsilon_f^l = -\frac{E_Y^f t^f \varepsilon_f}{\sum_i E_Y^i t^i}, \tag{10}$$

where E_Y^f and E_Y^i correspond to the Young's modulus of the ferroelectric layer and of every individual layer of the bending tongue, respectively. t^f corresponds to the thickness of the ferroelectric layer of the bending tongue.

The in-plane built-in and ferroelectric strains also generate a bending moment due to a net force created in each individual layer and acting through a moment arm spanning from the mid-plane of the layer, n^i (see Eq. 3), to the neutral axis of the bending tongue with the equivalent cross-section, n_{eff} (see Eq. 2).[20] The bending moment due to the built-in strain, M_b, and the one due to the ferroelectric strain M_f, arising from the forces acting in each layer due to ε_b^l and to ε_f^l, respectively, as well as to the forces acting in the ferroelectric layer due to ε_b and to ε_f, respectively, are expressed as:

$$\begin{aligned} M_b &= \sum_i E_Y^i t^i w_{eff}^i (n^i - n_{eff}) \varepsilon_b^l \sin(\theta) \\ &\quad + E_Y^{ferro} t^{ferro} w_{eff}^{ferro} (n^{ferro} - n_{eff}) \varepsilon_b \sin(\theta), \\ M_f &= \sum_i E_Y^i t^i w_{eff}^i (n^i - n_{eff}) \varepsilon_f^l \sin(\theta) \\ &\quad + E_Y^{ferro} t^{ferro} w_{eff}^{ferro} (n^{ferro} - n_{eff}) \varepsilon_f \sin(\theta), \end{aligned} \tag{11}$$

where the superscript *ferro* refers to the ferroelectric layer and θ refers to the angle between the in-plane force due to the strain and the moment arm. If the mid-plane of a layer, n^i, is located above the effective neutral axis of the bending tongue, n_{eff}, then $\theta = -90°$ and if n^i is smaller than n_{eff} then $\theta = 90°$.

The bending moment M_b, due to the built-in strain, is acting over the whole length of the bending tongue while M_f, due to the ferroelectric strain, is acting over the bending tongue's length minus the *length load*. The distribution of these bending moments, M(x), is described by the following equation using Macaulay brackets:

$$M(x) = M_b + M_f(1 - < x - m >^0). \tag{12}$$

According to Euler-Bernoulli beam theory, integrating twice the equation for the bending moment's distribution due to ε_b and ε_f gives the corresponding equation for the vertical deflection. It can be obtained from Eq. 12 and 8:

$$Z = \frac{1 - \nu_{eff}^2}{2E_Y^{eff} I_{eff}} [(M_b + M_f)x^2 - M_f < x - m >^2]. \tag{13}$$

The detailed calculations from Eq. 12 to Eq. 13 are given in Appendix B.

Both the built-in strain and the ferroelectric strain are dependent on the crystallographic state of the ferroelectric layer (polycrystalline, textured or epitaxial). Therefore, it is necessary to describe the crystallographic state mathematically.

1. Mathematical formulation of the crystallographic state

Following Hwang's model[8] for ferroelectric switching, the orientation of each crystallographic grain has an impact on the global ferroelectric strain and should therefore be taken into account. For this purpose, a series of systems of local coordinates defined relative to the *global reference frame* and referred to as *grain coordinates*, is defined.

The orientation of each grain is set by a group of three Euler angles, $\varphi_1, \phi, \varphi_2$, allowing conversion of coordinates from the *global reference frame* to the *grain coordinates* of each grain. As various conventions exist to define the Euler angles, the one chosen here is described below and represented in Fig. 2.

The first rotation of angle φ_1 around the z-axis creates the u-axis and v-axis in the xy-plane. The second rotation is made around the v-axis with an angle of ϕ. It creates the w-axis as well as the z'-axis. The third rotation occurs around the z'-axis with an angle of φ_2 and creates the x'-axis and the y'-axis. The *grain coordinates* of each grain are expressed in the reference frame made by the x'-axis, y'-axis and z'-axis.

These three successive rotations are described by the transformation matrix allowing to express the *grain coordinates* in the *global reference frame* as shown in the following equation:

$$\begin{pmatrix} x' \\ y' \\ z' \end{pmatrix} = \begin{pmatrix} k_{1,1} & k_{1,2} & k_{1,3} \\ k_{2,1} & k_{2,2} & k_{2,3} \\ k_{3,1} & k_{3,2} & k_{3,3} \end{pmatrix} \begin{pmatrix} x \\ y \\ z \end{pmatrix}, \tag{14}$$

where $k_{g,h}$ corresponds to the coefficients of the transformation matrix with g and h taking the values 1, 2 or 3.

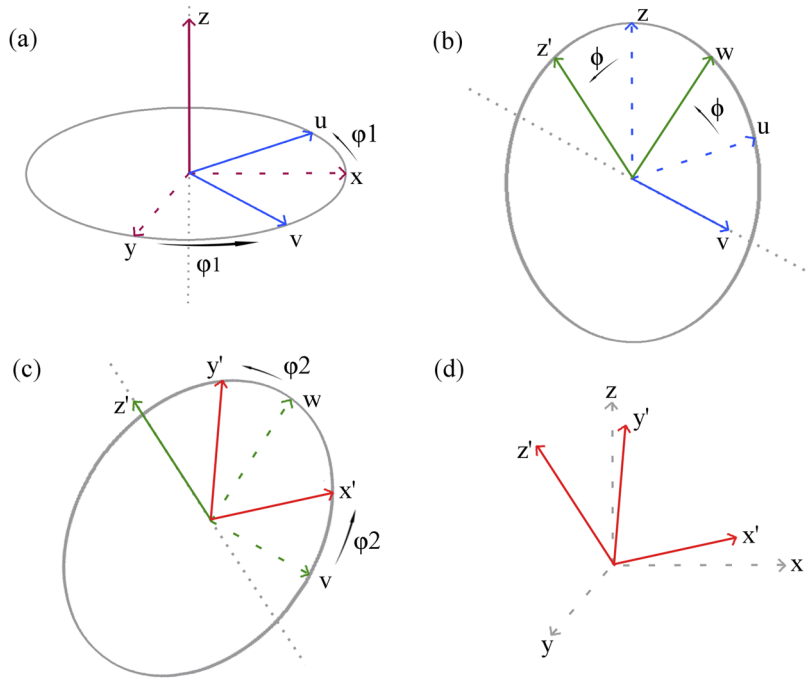

FIG. 2. Schematic representation of the three Euler angles to convert coordinates from the *global reference frame* to the *grain coordinates* of each grain. (a) *global reference frame* defined by the vectors *x*, *y* and *z* with the first rotation of angle φ_1 around the *z*-axis, (b) second rotation of angle ϕ around the *v*-axis, (c) third rotation of angle φ_2 around the *z'*-axis and (d) representation of the *global reference frame* and the *grain coordinates* defined by the vectors *x'*, *y'* and *z'*.

The coefficients $k_{g,h}$ are given in the following equation:

$$\begin{aligned}
k_{1,1} &= \cos(\varphi_1)\cos(\varphi_2) - \sin(\varphi_1)\sin(\varphi_2)\cos(\phi),\\
k_{1,2} &= -\sin(\varphi_2)\cos(\varphi_1) - \cos(\phi)\sin(\varphi_1)\cos(\varphi_2),\\
k_{1,3} &= \sin(\phi)\sin(\varphi_1),\\
k_{2,1} &= \cos(\varphi_2)\sin(\varphi_1) + \cos(\phi)\cos(\varphi_1)\sin(\varphi_2),\\
k_{2,2} &= -\sin(\varphi_2)\sin(\varphi_1) + \cos(\phi)\cos(\varphi_1)\cos(\varphi_2),\\
k_{2,3} &= -\sin(\phi)\cos(\varphi_1),\\
k_{3,1} &= \sin(\phi)\sin(\varphi_2),\\
k_{3,2} &= \sin(\phi)\cos(\varphi_2),\\
k_{3,3} &= \cos(\phi).
\end{aligned} \tag{15}$$

The Euler angles inherent to the grains are defined according to the three possible crystallographic states of the modelled ferroelectric strain. If the sample is polycrystalline, then all grains of the ferroelectric are randomly oriented and, therefore, the values of the three Euler angles are each randomly defined within their bounds ($0 < \varphi_1 < 2\,\pi$; $0 < \phi < \pi$ and $0 < \varphi_2 < 2\,\pi$).

In the case of a textured ferroelectric layer, a given percentage of grains are rotated by a few degrees around a given orientation, O, while the remaining grains are randomly oriented. The distribution of grains around the orientation O can be simulated by the following Gaussian function:[21]

$$S(\Psi) = \frac{8\sqrt{\pi}}{Z\Psi_0^3}\exp\left(\frac{-\Psi^2}{\Psi_0^3}\right), \tag{16}$$

where Ψ is the rotation angle around the orientation O, Ψ_0 is the full width at half-maximum of the Gaussian distribution and Z is the multiplicity due to the symmetry of the crystallographic unit cell.

Once normalized, the Gaussian distribution given in Eq. 16 contains 99.9% of the grains oriented around the orientation O between – 3Ψ and + 3Ψ. The distance between these two angles is separated into 10 segments, each containing a number of grains as defined by the Gaussian distribution. The grains contained in each segment are rotated by the average angle of the given segment around the orientation O.

If the ferroelectric layer is textured in-plane, the angle of rotation is the first Euler angle, φ_1, while ϕ and φ_2 are set to 0°. In the case of an out of plane texture, it is the second Euler angle, ϕ, which corresponds to the angle of rotation while φ_1 and φ_2 are set to 0°. A combination of in-plane and out-of-plane texture can be described by simultaneous rotations of φ_1 and ϕ.

The remaining grains which do not display texture around the orientation O are modelled by applying random values to their three Euler angles, as it is the case for a polycrystalline ferroelectric.

In this model, epitaxy is defined as the perfect alignment of grains in a given orientation O. Therefore, if the ferroelectric layer is epitaxial, all Euler angles are set to 0°, independent of any possible long range order between ferroelectric layer and substrate.

2. Built-in strain

The built-in strain in the ferroelectric layer, ε_b, is the sum of the thermal strain and the misfit strain. The choice of equation to calculate the former is dependent on the thickness of the thin film. The equation for the latter is

dependent on both the thin film thickness and its crystallographic state.

The thickness of the thin film mainly impacts the ability of the ferroelectric layer to relax. As the nature (strain, morphology, etc.) of the modelled thin film is unknown, its relaxation threshold should be determined and the corresponding equations should be used.

If the ferroelectric is not relaxed, its thermal strain, $\varepsilon_b^{thermal}$, due to cooling down from its deposition temperature, T_{depo}, to the bending tongue's operating temperature, T_{oper}, is expressed by:

$$\varepsilon_b^{thermal} = (T_{depo} - T_{oper}) * (\alpha^{subs} - \alpha^{ferro}), \tag{17}$$

where α corresponds to the thermal expansion coefficient.

If the ferroelectric layer is relaxed, the bi-axial stress present at Curie temperature, T_{Curie}, is partially released through the development of a domain structure.[22] The transformation stress concept implies that the thermal strain of a relaxed ferroelectric layer is described by:[23]

$$\varepsilon_b^{thermal} = (T_{depo} - T_{Curie}) * (\alpha^{subs} - \alpha^{ferro}). \tag{18}$$

Regarding the misfit strain, polycrystalline films are relaxed. For non-relaxed epitaxial ferroelectric films the misfit strain, ε_b^{misfit}, is described by:

$$\varepsilon_b^{misfit} = \left(\frac{a^{buffer} - a^{ferro}}{a^{ferro}}\right)_{T_{depo}}, \tag{19}$$

where a refers to the lattice parameter used for misfit strain calculation and the superscript *buffer* refers to the buffer layer adjacent to the ferroelectric layer.

If the ferroelectric layer is textured and not relaxed, its misfit strain is calculated from Eq. 19 and is multiplied by the percentage of textured grains.

In all of the above mentioned cases, the total strain can be reduced by a given degree of relaxation to model any further relaxation which could happen after the ferroelectric layer deposition.

3. Ferroelectric strain

The ferroelectric strain originates from both the ferroelectric switching strain component and the linear strain component. Hwang's model[8] processes each grain individually before averaging the ferroelectric strain and polarization values over the number of grains modelled. This individual processing of the grains imposes the need to work in *grain coordinates*. Therefore, every value in the *global reference frame* should be converted into *grain coordinates* through the use of Euler angles. Once the ferroelectric strain and matching polarization values are known for each individual grain, they should be converted back into the *global reference frame* before averaging.

Each grain is treated as if it is composed of unit cells displaying the same behavior (*i.e.* the same orientation relative to the *global reference frame*, simultaneous ferroelectric switching, etc.) and, therefore, *grain* can be replaced by *unit cell* for ease of comprehension.

Hwang *et al.* considered the sum of the electrical and mechanical work resulting from switching the polarization from its current direction to another one. Ferroelectric switching occurs if the applied electrical field is larger than a switching criterion expressed by:[8]

$$E\Delta P + \sigma\Delta\varepsilon_{int} > 2P_{spontaneous}E_{coercive}, \tag{20}$$

where E and σ correspond to the electrical field and to the stress, respectively, applied to the ferroelectric during the switching process. ΔP and $\Delta\varepsilon_{int}$ refer to the difference between before and after ferroelectric switching for the polarization and internal unit cell strain values, respectively. $P_{spontaneous}$ refers to the spontaneous polarization of the ferroelectric and $E_{coercive}$ refers to its coercive field.

According to Hwang's model, the polarization vector is parallel to the edge of the tetragonal unit cell. In our model, the polarization vector lies at the center of the unit cell and can only take six different orientations which is in agreement with Hwang's model. The six possible orientations of the polarization in a tetragonal perovskite ferroelectric, labelled from 1 to 6, are expressed in *grain coordinates* as [100], [$\bar{1}$00], [010], [0$\bar{1}$0], [001] and [00$\bar{1}$], respectively.

The internal unit cell strain values correspond to the elongation or the contraction of the cubic unit cell into the tetragonal one. These values are expressed as a function of strain along the unit cell a-axis, ε_a, or along its c-axis, ε_c. These two quantities are defined by:

$$\begin{aligned} \varepsilon_a &= \frac{a^{tetragonal} - a^{cubic}}{a^{cubic}}, \\ \varepsilon_c &= \frac{c^{tetragonal} - a^{cubic}}{a^{cubic}}, \end{aligned} \tag{21}$$

where a and c refer to the lattice parameters of the ferroelectric unit cell. The crystal system is indicated by the superscript, either *tetragonal* or *cubic*.

The internal unit cell strains inherent to the polarization orientations from 1 to 6 are [ε_c, ε_a, ε_a], [ε_c, ε_a, ε_a], [ε_a, ε_c, ε_a], [ε_a, ε_c, ε_a], [ε_a, ε_a, ε_c] and [ε_a, ε_a, ε_c], respectively.

From the values of the polarization orientations and of the internal unit cell strains, it can be noted that 180° ferroelectric switching would give rise to electrical work only while 90° switching would give rise to both electrical and mechanical work if dynamic poling is ignored.[24]

If several switching cases are possible for the same grain, *i.e.* the work associated with several switching events between the current polarization direction and a resulting one are larger than Hwang's switching criterion (see Eq. 20), then switching occurs in the direction resulting in the largest possible work.

The stress σ applied on the ferroelectric layer which is used to calculate the mechanical work is the one inherent to the built-in strain ε_b described in section III B 2. According to the assumptions stated in section II B, the ferroelectric material is a linear, homogeneous and isotropic material. In this case:

$$\begin{aligned}\varepsilon_b^x &= \varepsilon_b,\\ \varepsilon_b^y &= \varepsilon_b^x,\\ \varepsilon_b^z &= -\frac{\varepsilon_b^x}{\nu^{ferro}},\end{aligned} \tag{22}$$

where the superscripts x, y and z correspond to the directions in which the built-in strain is expressed in the *global reference frame*.

By combining Eq. 22 with Hooke's law for a linear, homogeneous and isotropic material, it yields:

$$\begin{aligned}\sigma^x &= 0,\\ \sigma^y &= 0,\\ \sigma^z &= E_Y^{ferro}\frac{2\nu^{ferro} - \frac{1}{\nu^{ferro}} + 1}{(1+\nu^{ferro})(1-2\nu^{ferro})}\varepsilon_b^x.\end{aligned} \tag{23}$$

The electrical field applied to the ferroelectric layer which is used to calculate the electrical work depends on which one of the four states of the bending tongue is being modelled (see section II A). While the states *as deposited* and *inactive* are not subjected to any electrical field, the states *poled* and *active* are subjected to the poling and applied electrical fields, respectively.

The ferroelectric switching strain corresponds to the average of the strain resulting, in the *global reference frame*, from Hwang's switching criterion method. The second component of the ferroelectric strain is the linear strain in the xy-plane, ε_f^{linear}, described by:

$$\varepsilon_f^{linear} = Ed_{31}, \tag{24}$$

where E is the applied electrical field along the z-axis and d_{31} is the piezoelectric coefficient linking E and the strain along the x-axis.

While Hwang's model allows the calculation of the ferroelectric strain, it has two severe limitations: the saturation of the linear ferroelectric strain is not taken into account and the remanent strain is calculated empirically. The model here described proposes a solution to these two points.

From Hwang's model the polarization can be plotted versus the applied electrical field, E. It is possible to determine the applied field at which saturation is reached, E^{sat}, as the point where the PE *loop* closes. This point is located on loops subsequent to the poling step, when the respective values of E and polarization are equal on the branches of increasing and decreasing applied field.

Once the value of the applied electrical field at which saturation is reached is known, all further calculations can be adapted by replacing E with E_{sat} in Eq. 24 once E becomes larger than E_{sat}. This approach generates underestimated strain values above saturation, which is more relevant for applications than neglecting saturation.

It is also possible, by plotting the ferroelectric strain ε_f versus the applied electrical field E, to obtain the remanent strain which corresponds to the value of ε_f at E = 0, after the poling step.

In summary, the bending tongue is subjected to the ferroelectric switching and linear strains in the *poled* state, to the remanent strain in the *inactive* state and to the remanent and linear strains in the *active* state. This is due to the fact that during operation the bending tongue is driven between the *inactive* and *active* states which does not cause any ferroelectric switching.

IV. RESULTS AND DISCUSSION

Unless otherwise mentioned, the results given hereafter correspond to the modelling[37] of a bending tongue composed of stainless steel 304 as a substrate, $LaNiO_3$ as a buffer layer and $PbZr_{0.52}Ti_{0.48}O_3$ for the ferroelectric layer. The layers have thicknesses of 100 μm, 0.004 μm and 1 μm, respectively. The modelled bending tongue has a length of 7 mm, a width of 3 mm and is subjected to a load of $5 \cdot 10^{-5}$ N applied over 1 mm at its free end. The $PbZr_{0.52}Ti_{0.48}O_3$ layer is epitaxial and has the density of tetragonal PZT, as assumed in the model. The applied electrical field is 500 kV·cm^{-1}. The modelling parameters used for the physical and mechanical properties of the ferroelectric, buffer and substrate layers are given in Table I.[25–36]

A polarization versus applied electrical field curve, or PE *loop*, has been modelled in Fig. 3 for an epitaxial and a polycrystalline $PbZr_{0.52}Ti_{0.48}O_3$ layer. It can be noted that the polycrystalline PE *loop* is rounded and wider than the epitaxial one, which is more square-shaped. Indeed, due to the random orientation of grains in the polycrystalline layer, the alignment of each grain polarization towards the applied field direction is progressive. Each grain perceives the applied electrical field differently due to its own orientation.

The sharp ferroelectric PE *loop* for the epitaxial case, on the other hand, is due to the perfect alignment of all grains. As they perceive the applied electrical field in the same manner, they answer to it simultaneously.

Furthermore, in the epitaxial PE *loop* the poling appears as a two steps process. 180° ferroelectric switching occurs at a lower applied field (at 175 kV·cm^{-1}) than 90° switching which occurs at 360 kV·cm^{-1}. This phenomenon is consistent with the modelling of the ferroelectric strain described in section III B 3: as 180° switching is only due to electrical work, it requires less energy than 90° switching, which is due to both electrical and mechanical work. Indeed, while both 180° and 90° switching involve a change in polarization, 90° switching also implies a change in strain. The tetragonal unit cell is deformed, shortening along its c-axis and elongating along its a-axis, effectively inverting its a-axis and its c-axis.

Once the individual polarization of each grain has been switched and aligned as closely as possible with the applied field direction, only 180° switching remains.

Both epitaxial and polycrystalline PE *loops* are shifted towards the right-hand side of the graph by 53 kV·cm^{-1}. This shift is due to the built-in strain (thermal and eventual misfit strains) which generates stress on the ferroelectric layer, impacting the mechanical work required to switch the polarization of a given grain (see Eq. 20,23).

TABLE I. Physical and mechanical properties of materials used for modelling. Ferroelectric material: $PbZr_{0.52}Ti_{0.48}O_3$; Buffer layer: $LaNiO_3$ and Substrate: stainless steel 304 (EU: 1.4301).

	Parameter	Value
Ferroelectric layer	Young's modulus[25]	$9.9 \cdot 10^{10}$ Pa
	Poisson's ratio[26]	0.31
	Coercive field[27]	$1.5 \cdot 10^{7}$ V.m^{-1}
	Spontaneaous polarization[28]	0.5 C.m^{-2}
	Piezoelectric coefficient d_{31}[29]	$-97 \cdot 10^{-12}$ V.m^{-1}
	Lattice parameter tetragonal a[30]	$4.043 \cdot 10^{-10}$ m
	Lattice parameter tetragonal c[30]	$4.132 \cdot 10^{-10}$ m
	Lattice parameter cubic a (above Curie temperature)[31]	$4.085 \cdot 10^{-10}$ m
	Thermal expansion coefficient[32]	$2 \cdot 10^{-6}$ K^{-1}
	Curie temperature[29]	573 K
	Density[29]	7600 kg.m^{-3}
Buffer layer	Young's modulus[33]	$5.63 \cdot 10^{7}$ Pa
	Lattice parameter for epitaxial strain calculation[34]	$3.851 \cdot 10^{-10}$ m
	Density[34]	7141 kg.m^{-3}
Substrate	Young's modulus[35]	$2.0 \cdot 10^{11}$ Pa
	Poisson ratio[36]	0.27
	Thermal expansion coefficient[35]	$16.5 \cdot 10^{-6}$ K^{-1}
	Density[35]	7900 kg.m^{-3}

Besides the poling step from 0 to 450 kV·cm^{-1}, the *PE loops* have been plotted by decreasing the applied field to -450 kV·cm^{-1} and subsequently increasing it to 450 kV·cm^{-1} three consecutive times. In the case of the epitaxial PE loop, only one trace can be seen from these three consecutive loops. Hence, the epitaxial ferroelectric displays reproducible behavior.

In the case of the polycrystalline *PE loop*, two traces can be seen while the applied electrical field is decreasing:

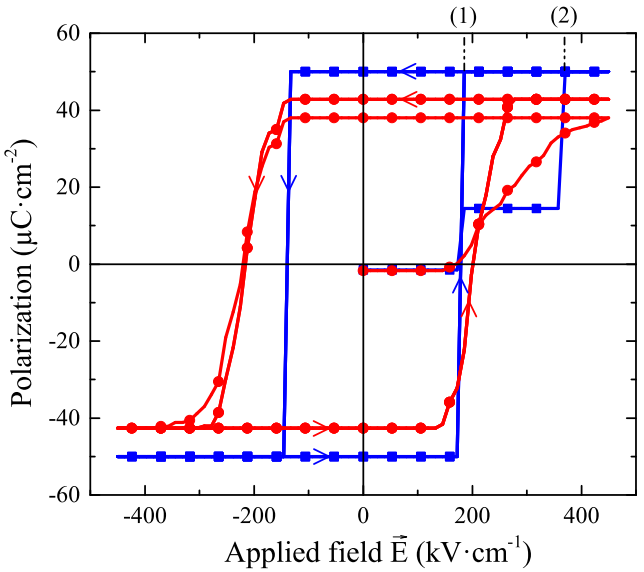

FIG. 3. Modelled polarization versus applied electrical field curve in the case of an epitaxial (blue squares) and of a polycrystalline (red circles) ferroelectric layer. (1) and (2) indicate 180° and 90° switching of the epitaxial film, respectively.

one starting from the poling step and one from the first branch where the applied field increases. This originates from the random alignment of the grains in the polycrystalline sample: as they do not all perceive the applied field in the same manner due to their own orientation, the electrical work is different from one grain to the other. Some grains might not have had enough energy during the poling step to switch and align their polarization with the applied field direction. In this case, the ferroelectric switching might be more favorable when the applied field is oriented in the opposite direction. It can be noticed, that once the field has been increased (through the poling step) and decreased once, the second and third *PE loops* are identical indicating that all grains are switching when the applied field direction is reversed.

The grain orientation also impacts the bending tongue's vertical deflection as can be seen in Fig. 4. Based on the definition of the crystallographic state given in section III B 1, a polycrystalline ferroelectric should behave the same way as a 0% textured one while an epitaxial ferroelectric should behave identically to a 100% textured one, which is confirmed by the simulation.

It can be noted that the polycrystalline sample displays a slightly negative vertical deflection of – 1.96 μm while every bending tongue modelled with either textured or epitaxial ferroelectric bends upwards. The ferroelectric strain being smaller than in the other cases, the deflection is determined by the other terms (*e.g.* the bending tongue's own weight or the load applied at its free end) which are bending the bending tongue downwards.

The strain versus applied electrical field curve, or *butterfly loop*, is represented in Fig. 5. It displays the ferroelectric strain saturation and the remanent strain, characteristic of ferroelectric behavior. Along with the hysteretic behavior

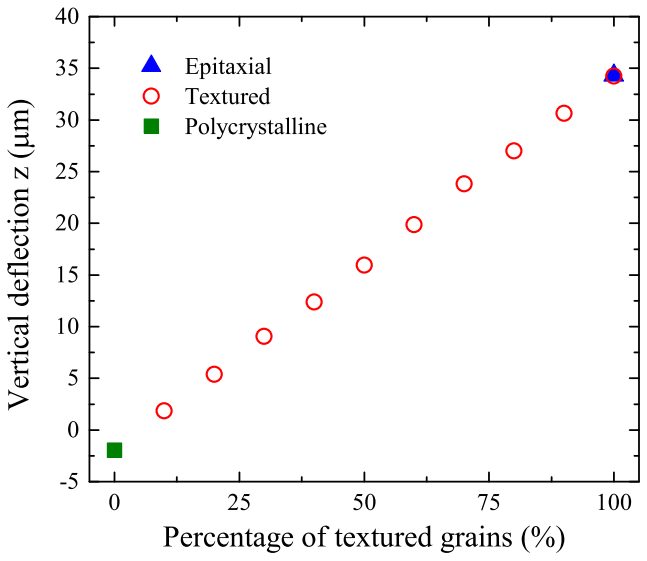

FIG. 4. Evolution of the vertical deflection as a function of the percentage of textured grains. The case of an epitaxial and a polycrystalline ferroelectric layer are shown for comparison.

shown in the *PE loops*, it proves that ferroelectrics are properly modelled.

It should be noted that the strain in the z direction, ε^z, is calculated through:

$$\varepsilon^z = -\frac{\varepsilon_f}{\nu^{ferro}}, \tag{25}$$

and corresponds to the ferroelectric strain in the bending tongue perpendicular to its surface. The vertical deflection is obtained through the equations of section III for the corresponding strain values of the *butterfly loop*.

The lack of symmetry in the *butterfly loop* is due to the built-in strain, generating stress on the ferroelectric layer, similar to the *PE loops*.

Two key elements of the *butterfly loop*, which were not present in Hwang's model, are the saturation of the ferroelectric strain, clearly visible, and the remanent strain. The modelled ferroelectric saturates at 3.73% strain, equivalent to 34.9 μm of vertical deflection. This last value is essential for applications as it defines the maximum vertical deflection of the bending tongue. The modelled remanent strain, 3.15%, is 3.8 times larger than the empirical remanent strain calculated from Hwang *et al.*[8] This is due to the built-in strain, constraining the ferroelectric layer, which has not been taken into account by Hwang's model.

The respective contributions of the bending tongue's own weight, the load applied at its free end, the built-in and the ferroelectric strains to the vertical deflection, *z*, are shown in Fig. 6. In the given example, under an applied field of 500 kV·cm^{-1}, the main contribution comes from the ferroelectric strain. The built-in strain, load at the bending tongue's free end and its weight account for 4.47%, 0.61% and 0.36% of the vertical deflection due to the ferroelectric strain, respectively. However, as these three terms are deflecting the bending tongue downwards opposing the ferroelectric strain, the sum of all terms is smaller than the vertical deflection due to the ferroelectric strain.

The relative importance of each contribution is strongly dependent on the parameters chosen for the modelling. While

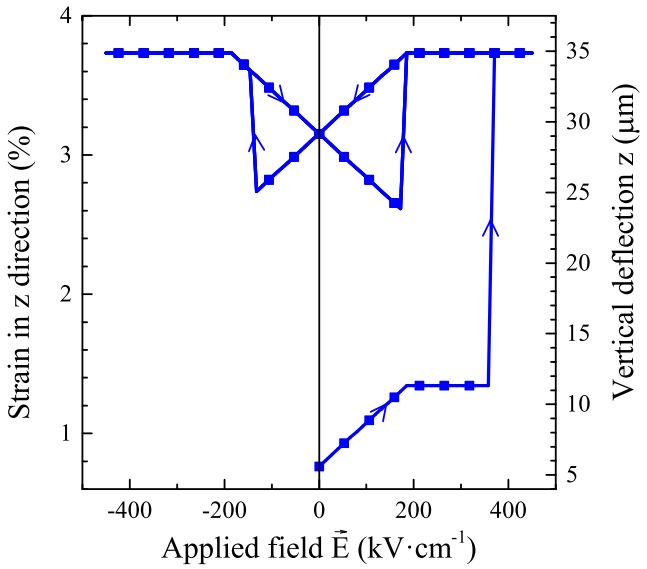

FIG. 5. Modelled strain versus applied electrical field curve and vertical deflection versus applied electrical field curve in the case of an epitaxial ferroelectric layer.

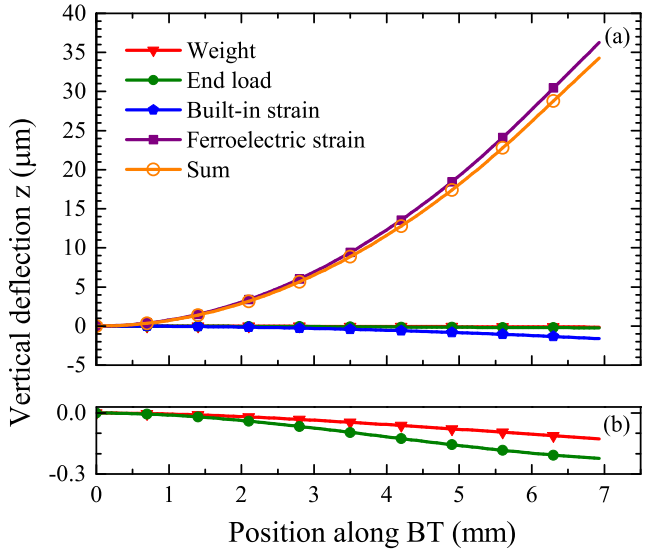

FIG. 6. Contribution to the vertical deflection of the bending tongue (BT). (a) individual contributions from weight, end load, built-in strain and ferroelectric strain as well as sum of all contributions, (b) weight and end-load individual contributions.

all parameters (*i.e.* materials related or geometrical) can be varied in the proposed model, a set of relevant parameters is being varied in the following examples to discuss their impact. The applied electrical field is kept constant at 500 kV·cm^{-1} to model results at saturation.

A crucial component of the bending tongue is the ferroelectric layer, its thickness being decisive for the vertical deflection, as shown in Fig. 7(a). In the given example, the vertical deflection which can be reached, z, increases almost proportionally to the thickness of the ferroelectric layer. As the ferroelectric thickness increases from 0.2 μm to 2.0 μm, the vertical deflection increases from $z = 6.7\ \mu m$ to $z = 67.2\ \mu m$.

While the vertical deflection is important for applications, the variation in vertical deflection between the *active* state (where an electrical field $\vec{E}$ is applied) and the *inactive* state (where no electrical field is applied) is the key to the accessible range of motion of the bending tongue. For the modelled example, it ranges from $z^E - z^0 = 1.1\ \mu m$ to $z^E - z^0 = 10.9\ \mu m$ when the ferroelectric thickness is increased from 0.2 μm to 2.0 μm.

On the other hand, the vertical deflection is not proportional to the length of the bending tongue, as can be seen in Fig. 7(b). The vertical deflection increases from $z = 2.1\ \mu m$ to $z = 266.1\ \mu m$ as the length is extended from 2 mm to 20 mm. The most important result is once more the variation in vertical deflection between the *active* state and the *inactive* state, reaching $z^E - z^0 = 0.4\ \mu m$ at a length of 2 mm and $z^E - z^0 = 46.8\ \mu m$ at a length of 20 mm. The length of the bending tongue, if not restricted in a given application, is therefore an interesting parameter to increase the vertical deflection.

Other parameters also impact the vertical deflection, like the load applied at the free end as represented in Fig. 7(c). As the end load increases from 0 mN to 10 mN, the bending tongue's deflection is inverted from upwards to downwards. This corresponds to the increase of the end load component relative to the ferroelectric component up to the point where it becomes the dominant component of deflection. The critical point at which the direction of the deflection is inverted is reached at an end load of 7.8 mN.

Increasing the load applied at the free end of the bending tongue does not impact the variation in vertical deflection between the *active* state and the *inactive* state, which is determined mostly by the ferroelectric layer thickness and the bending tongue's length.

It should be noted that some of the parameters impact the vertical deflection in various ways through Eq. 9 and 13. This is the case for the geometrical dimensions of the bending tongue (length, width, thicknesses of the layers and *length load*), which are parameters of both the bending tongue's own weight and its effective second moment or area, I_{eff}. This is particularly relevant for the length and *length load* as these two parameters are further involved into the equations of vertical deflection (Eq. 9 and 13).

Other parameters, while having a global impact on the bending tongue's vertical deflection, impact all terms of the

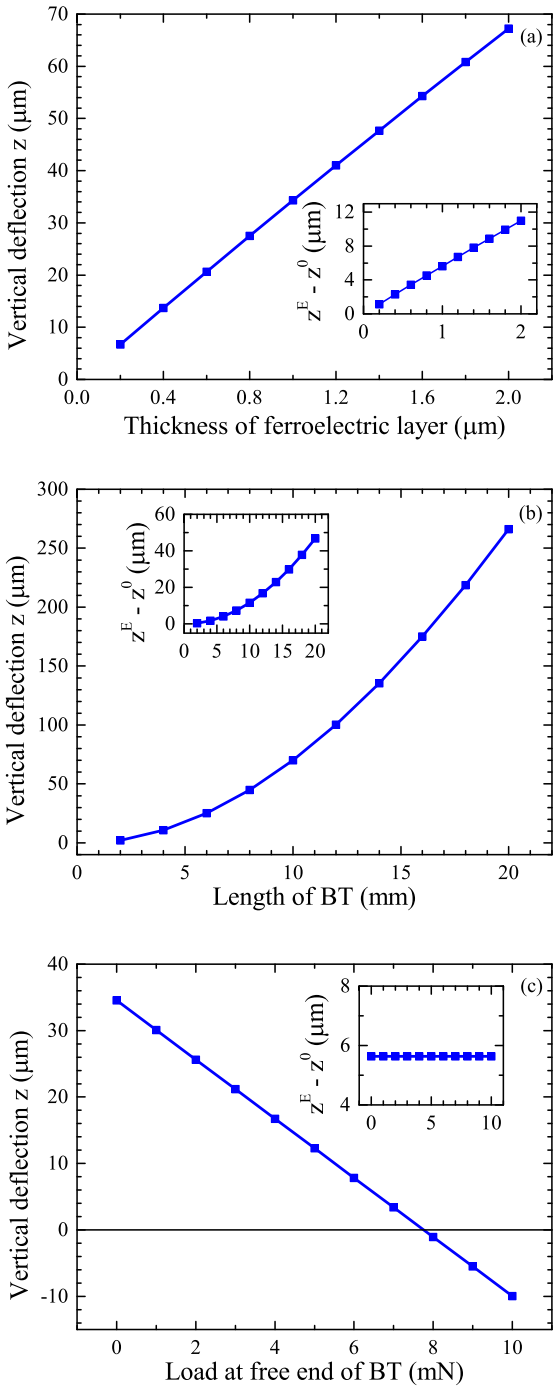

FIG. 7. Evolution of the vertical deflection as a function of (a) the ferroelectric layer thickness with a length of 7 mm and a load at its free end of $5 \cdot 10^{-5}$ N, (b) the length of the bending tongue (BT) with a ferroelectric layer thickness of 1 μm and a load at its free end of $5 \cdot 10^{-5}$ N and (c) the load at its free end with a length of 7 mm and a ferroelectric layer thickness of 1 μm. $z^E - z^0$ represents the variation in vertical deflection between the *active* state (where an electrical field $\vec{E}$ is applied) and the *inactive* state (where no electrical field is applied). As $\vec{E}$ is kept constant at 500 kV·cm^{-1}, saturation is reached.

deflection (the bending tongue's own weight, the load applied at its free end, the built-in and the ferroelectric strains to the vertical deflection) in an almost similar manner, maintaining the relative proportions between them. For example, the Young's moduli of the materials are mostly taken into account at the forefront of Eq. 9 and 13, effectively impacting all the terms of the deflection. However, these parameters will also have some minor impact on the built-in and ferroelectric strains (see Eq. 10,11 and 23). The same behavior is visible with the Poisson's ratios of the materials.

Finally, some parameters impact a single component of the vertical deflection. It is the case for the materials densities, which affect only the weight component, as well as for the piezoelectric coefficient, d_{31}, and the applied electrical field, which influences only the ferroelectric strain component.

Any built-in strain parameter, like the operating and deposition temperatures, texture parameters, thermal expansion coefficients and lattice parameters of the materials, necessarily influence the ferroelectric strain. This occurs through the stress generated by the built-in strain on the ferroelectric layer, which influences the ferroelectric switching (see Eq. 23).

When working towards applications, the main advantage of this large array of parameters resides in the tunability of the bending tongue modelling. Indeed, it is possible to fix a set of parameters based on constraints of the application and to adapt the other parameters to reach the chosen range of vertical deflection.

For example, it is possible to study the impact of the load applied at the free end of the bending tongue on the maximum vertical deflection at the free end. If this load, considered only in Eq. 9, is the only parameter which can be varied, the deflection at the bending tongue's free end, in $x = l$, can be expressed as:

$$\Delta Z = \Delta q^L \frac{1-\nu_{eff}^2}{24 E_Y^{eff} I_{eff}} (3l^4 - 4\, m^3 l + m^4), \tag{26}$$

where ΔZ and Δq^L are the variations in the vertical deflection and the load applied at the free end of the bending tongue, respectively.

Therefore, if the bending tongue's length, the ferroelectric layer thickness and the load at the free end are fixed, it is possible to calculate the maximum end load to reach a chosen vertical deflection.

This analysis can be performed for any parameter, giving insight into the respective impact of each parameter and allowing optimization of the bending tongue when some parameters are constrained by the application.

V. CONCLUSIONS

The proposed modelling of ferroelectric bending tongues gives access to the vertical deflection while taking ferroelectric switching on the grain scale into account. The proper modelling of ferroelectric switching can be verified through the *PE loop* and the *butterfly loop*, both displaying hysteretic behavior and saturation.

The description of the saturation in the *butterfly loop* is an improvement of Hwang's model on which the description of ferroelectric switching is based. This addition is crucial for applications were the maximum accessible deflection and the corresponding applied electrical field required to reach it are needed.

Additional features have been added, notably the calculation of the remanent strain and the impact of the crystallographic state of the ferroelectric (polycrystalline, textured or epitaxial).

The large amount of parameters taken into account in this model allows the relative importance of the contributions to the vertical deflection (bending tongue's own weight, load applied at its free end, built-in and ferroelectric strains) to be ascertained and the bending tongue's geometry to be optimized. As the materials properties cannot be changed easily, the geometry of the bending tongue optimization is essential for specific applications.

ACKNOWLEDGMENTS

This work was funded by the Deutsche Forschungsgemeinschaft (DFG) under the grant number AL 560/19-1.

A travel grant from the EIT RawMaterials IDS-FunMat-Inno is also acknowledged.

We acknowledge support by the German Research Foundation and the Open Access Publishing Fund of Technische Universität Darmstadt.

APPENDIX A: DEVELOPMENT FROM THE LOAD DISTRIBUTION (EQ. 6) TO THE EQUATION OF VERTICAL DEFLECTION DUE TO LOADS (EQ. 9)

The load distribution on the bending tongue is described by Eq. 6, using Macaulay brackets. According to Euler-Bernoulli beam theory, it can be written:

$$EI * Z^{IV} = q^W + q^L < x - m >^0 . \tag{A1}$$

It is necessary to take into account the corrections of the beam inhomogeneity through E_Y^{eff} and I_{eff} (Eq. 4) and of its disproportionate width (Eq. 5). Therefore, Eq. A1 can be formulated as:

$$\frac{1-\nu_{eff}^2}{E_Y^{eff} I_{eff}} * Z^{IV} = q^W + q^L < x - m >^0 . \tag{A2}$$

Following Euler-Bernoulli beam theory, Eq. A2 should be integrated four consecutive times over the length of the bending tongue. The first integration yields:

$$\frac{1-\nu_{eff}^2}{E_Y^{eff} I_{eff}} * Z^{III} = q^W x + q^L < x - m >^1 + cst_1, \tag{A3}$$

where cst_1 is an integration constant. It can be calculated using the boundary conditions given in Eq. 8:

$$Z^{III}(x = l) = 0 \rightarrow cst_1 = -q^W l - q^L (l - m). \tag{A4}$$

By combining Eq. A3 and A4, it yields:

$$\frac{1-\nu_{eff}^2}{E_Y^{eff} I_{eff}} * Z^{II} = q^W \frac{x^2}{2} + \frac{q^L}{2} < x-m >^2 - [q^W l + q^L (l-m)]x + cst_2, \quad (A5)$$

where cst_2 is an integration constant. It can be calculated using the boundary conditions given in Eq. 8:

$$Z^{II}(x=l) = 0 \rightarrow cst_2 = q^W \frac{l^2}{2} + q^L (l-m)(-\frac{l-m}{2} + l). \quad (A6)$$

By combining Eq. A5 and A6, it yields:

$$\frac{1-\nu_{eff}^2}{E_Y^{eff} I_{eff}} * Z^{I} = q^W \frac{x^3}{6} + \frac{q^L}{6} < x-m >^3 - [q^W l + q^L (l-m)]\frac{x^2}{2} + [q^W \frac{l^2}{2} + q^L (l-m)(l - \frac{l-m}{2})]x + cst_3, \quad (A7)$$

where cst_3 is an integration constant. It can be calculated using the boundary conditions given in Eq. 8:

$$Z^{I}(x=0) = 0 \rightarrow cst_3 = 0. \quad (A8)$$

By combining Eq. A7 and A8, it yields:

$$\frac{1-\nu_{eff}^2}{E_Y^{eff} I_{eff}} * Z = q^W \frac{x^4}{24} + \frac{q^L}{24} < x-m >^4 - [q^W l + q^L (l-m)]\frac{x^3}{6} + [q^W \frac{l^2}{2} + q^L (l-m)(l - \frac{l-m}{2})]\frac{x^2}{2} + cst_4, \quad (A9)$$

where cst_4 is an integration constant. It can be calculated using the boundary conditions given in Eq. 8:

$$Z(x=0) = 0 \rightarrow cst_4 = 0. \quad (A10)$$

By combining Eq. A9 and A10, it yields:

$$Z = \frac{1-\nu_{eff}^2}{24 E_Y^{eff} I_{eff}} \left[q^W x^4 + q^L < x-m >^4 + 4(-q^W l - q^L (l-m))x^3 + 12\left[q^W \frac{l^2}{2} + q^L (l-m)\left(l - \frac{l-m}{2}\right)\right]x^2\right], \quad (A11)$$

corresponding to Eq. 9.

APPENDIX B: DEVELOPMENT FROM THE BENDING MOMENTS DUE TO STRAIN DISTRIBUTION (EQ. 12) TO THE EQUATION OF VERTICAL DEFLECTION DUE TO BENDING MOMENTS (EQ. 13)

The bending moments due to strain distribution on the bending tongue is described by Eq. 12, using Macaulay brackets. According to Euler-Bernoulli beam theory, it can be written:

$$EI * Z^{II} = M_b + M_f(1 - < x-m >^0). \quad (B1)$$

It is necessary to take into account the corrections of the beam inhomogeneity through E_Y^{eff} and I_{eff} (Eq. 4) and of its disproportionate width (Eq. 5). Therefore, Eq. B1 can be formulated as:

$$\frac{1-\nu_{eff}^2}{E_Y^{eff} I_{eff}} * Z^{II} = M_b + M_f(1 - < x-m >^0). \quad (B2)$$

Following Euler-Bernoulli beam theory, Eq. B2 should be integrated two consecutive times over the length of the bending tongue. The first integration yields:

$$\frac{1-\nu_{eff}^2}{E_Y^{eff} I_{eff}} * Z^{I} = (M_b + M_f)x - M_f < x-m >^1 + cst_5, \quad (B3)$$

where cst_5 is an integration constant. It can be calculated using the boundary conditions given in Eq. 8:

$$Z^{I}(x=0) = 0 \rightarrow cst_5 = 0. \quad (B4)$$

By combining Eq. B3 and B4, it yields:

$$\frac{1-\nu_{eff}^2}{E_Y^{eff} I_{eff}} * Z = (M_b + M_f)\frac{x^2}{2} - \frac{M_f}{2} < x-m >^2 + cst_6, \quad (B5)$$

where cst_6 is an integration constant. It can be calculated using the boundary conditions given in Eq. 8:

$$Z(x=0) = 0 \rightarrow cst_6 = 0. \quad (B6)$$

By combining Eq. B5 and B6, it yields:

$$Z = \frac{1-\nu_{eff}^2}{2E_Y^{eff} I_{eff}}[(M_b + M_f)x^2 - M_f < x-m >^2], \quad (B7)$$

corresponding to Eq. 13.

REFERENCES

[1] S. Trolier-McKinstry and P. Muralt, "Thin film piezoelectrics for MEMS," J. Electroceramics **12**, 7–17 (2004).
[2] R. G. Ballas, H. F. Schlaak, and A. J. Schmid, "The constituent equations of piezoelectric multilayer bending actuators in closed analytical form and experimental results," Sensors Actuators, A Phys. **130-131**, 91–98 (2006).
[3] R. G. Ballas, *Piezoelectric multilayer beam bending actuators*, 1st ed. (Springer, Berlin, 2007).
[4] L. Q. Chen, "Phase-field method of phase transitions/domain structures in ferroelectric thin films: A review," J. Am. Ceram. Soc. **91**, 1835–1844 (2008).

[5]Y. Su and C. M. Landis, "Continuum thermodynamics of ferroelectric domain evolution: Theory, finite element implementation, and application to domain wall pinning," J. Mech. Phys. Solids **55**, 280–305 (2007).
[6]B. X. Xu, D. Schrade, R. Müller, D. Gross, T. Granzow, and J. Rödel, "Phase field simulation and experimental investigation of the electro-mechanical behavior of ferroelectrics," ZAMM Zeitschrift fur Angew. Math. und Mech. **90**, 623–632 (2010).
[7]J. E. Huber, N. A. Fleck, C. M. Landis, and R. M. McMeeking, "A constitutive model for ferroelectric polycrystals," J. Mech. Phys. Solids **47**, 1663–1697 (1999).
[8]S. C. Hwang, C. S. Lynch, and R. M. McMeeking, "Ferroelectric/ferroelastic interactions and a polarization switching model," Acta Metall. Mater. **43**, 2073–2084 (1995).
[9]S. Hwang, J. Huber, R. McMeeking, and N. Fleck, "The simulation of switching in polycrystalline ferroelectric ceramics," J. Appl. Phys. **84**, 1530–1540 (1998).
[10]R. M. McMeeking and S. C. Hwang, "On the potential energy of a piezoelectric inclusion and the criterion for ferroelectric switching," Ferroelectrics **200**, 151–173 (1997).
[11]X. Chen, D. N. Fang, and K. C. Hwang, "Micromechanics simulation of ferroelectric polarization switching," Acta Mater. **45**, 3181–3189 (1997).
[12]W. Chen and C. S. Lynch, "A micro-electro-mechanical model for polarization switching of ferroelectric materials," Acta Mater. **46**, 5303–5311 (1998).
[13]S. Hwang and R. Waser, "Study of electrical and mechanical contribution to switching in ferroelectric/ferroelastic polycrystals," Acta Mater. **48**, 3271–3282 (2000).
[14]Y. Fotinich and G. P. Carman, "Stresses in piezoceramics undergoing polarization switchings," J. Appl. Phys. **88**, 6715–6725 (2000).
[15]J. Li and G. J. Weng, "A micromechanics-based hysteresis model for ferroelectric ceramics," J. Intell. Mater. Syst. Struct. **12**, 79–91 (2001).
[16]F. Narita, Y. Shindo, and K. Hayashi, "Bending and polarization switching of piezoelectric laminated actuators under electromechanical loading," Comput. Struct. **83**, 1164–1170 (2005).
[17]F. I. Baratta, "When is a beam a plate?," Commun. Am. Ceram. Soc. **64**, C-86 (1981).
[18]W. C. Young and R. G. Budynas, *Roark's formulas for stress and strain*, 7th ed. (McGraw-Hill Book Company, New York City, 2002), pp. 125–266.
[19]W. H. Macaulay, "Note on the deflection of beams," Messenger Math. **48**, 129–130 (1919).
[20]T. Bailey and J. E. Hubbard, Jr., "Distributed piezoelectric-polymer active vibration control of a cantilever beam," J. Guid. Control. Dyn. **8**, 605–611 (1985).
[21]K. Lücke, J. Pospiech, K. H. Virnich, and J. Jura, "On the problem of the reproduction of the true orientation distribution from pole figures," Acta Metall. **29**, 167–185 (1981).
[22]B. Tuttle, T. Headley, C. Drewien, J. Michael, J. Voigt, and T. Garino, "Comparison of ferroelectric domain assemblages in Pb(Zr,Ti)O_3 thin films and bulk ceramics," Ferroelectrics **221**, 209–218 (1999).
[23]C. B. Yeager and S. Trolier-McKinstry, "Epitaxial Pb(Zr_x,Ti_{1-x})O_3 (0.30 ≤ x ≤ 0.63) films on (100) MgO substrates for energy harvesting applications," J. Appl. Phys. **112**, 074107 (2012).
[24]S. Trolier-McKinstry, N. Bassiri Gharb, and D. Damjanovic, "Piezoelectric nonlinearity due to motion of 180° domain walls in ferroelectric materials at subcoercive fields: A dynamic poling model," Appl. Phys. Lett. **88**, 202901 (2006).
[25]Q. Sunder and Bakialakshmi, "Human energy harvesting based on piezoelectric transduction using MEMS technology," Int. J. Adv. Res. Electr. Electron. Instrum. Eng. **3**, 8958–8965 (2014).
[26]A. J. Fleming and K. K. Leang, *Design, modeling and control of nanopositioning systems* (2014), p. 21.
[27]N. A. Pertsev, J. Rodríguez Contreras, V. G. Kukhar, B. Hermanns, H. Kohlstedt, and R. Waser, "Coercive field of ultrathin *Pb*($Zr_{0.52}Ti_{0.48}$)O_3 epitaxial films," Appl. Phys. Lett. **83**, 3356–3358 (2003).
[28]M. J. Haun, E. Furman, S. J. Jang, and L. E. Cross, "Thermodynamic theory of the lead zirconate-titanate solid solution system, Part V: Theoretical calculations," Ferroelectrics **99**, 63–86 (1989).
[29]J. L. Butler and C. H. Sherman, *Transducers and arrays for underwater sound*, 2nd ed. (ASA Press, 2007) Chap. 13.
[30]International Centre for Diffraction (ICDD), "Powder diffraction file (PDF): 01-072-7167," *Pb*($Zr_{0.52}Ti_{0.48}$)O_3 @ 298 K (2013).
[31]International Centre for Diffraction (ICDD), "Powder diffraction file (PDF): 04-011-7309," *Pb*($Zr_{0.52}Ti_{0.48}$)O_3 @ 850 K (2013).
[32]S. N. Kallaev, G. G. Gadzhiev, I. K. Kamilov, Z. M. Omarov, S. A. Sadykov, and L. A. Reznichenko, "Thermal properties of PZT-based ferroelectric ceramics," Phys. Solid State **48**, 1169–1170 (2006).
[33]Y. H. Yu, M. O. Lai, L. Lu, and G. Y. Zheng, "Measurement of Young's modulus and Poisson's ratio of thin films by synchrotron x-ray diffraction," Adv. Synchrotron Radiat. **1**, 179–187 (2008).
[34]International Centre for Diffraction (ICDD), "Powder diffraction file (PDF): 04-007-6256," *La*NiO_3 @ 298 K (2013).
[35]Euro Inox- The European Stainless Steel Development Association, *Stainless steel: table of technical properties* (*Materials and Applications Series, Volume* 5), 2nd ed. (2007) p. 16.
[36]H. Rohloff and A. Zastera, *Physikalische Eigenschaften gebräuchlicher Stähle* (Verlag Stahleisen, Düsseldorf, 1996).
[37]Technische Universität Darmstadt - Institute of Materials Science - Advanced Thin Film Technology (ATFT), "FeBeTo - Ferroelectric bending tongues modelling program," <https://www.mawi.tu-darmstadt.de/ds> (2018).